Applied Catalysis B: Environmental 325 (2023) 122306

Contents lists available at ScienceDirect

Applied Catalysis B: Environmental

journal homepage: www.elsevier.com/locate/apcatb

Degradation of perfluorooctanesulfonate (PFOS) by sub-bandgap irradiation of hydrogen-terminated nanodiamond

William A. Maza *, Vanessa M. Breslin, Tatyana I. Feygelson, Paul A. DeSario, Bradford B. Pate, Jeffrey C. Owrutsky, Albert Epshteyn

Chemistry Division, Naval Research Laboratory, Washington D.C. 20375, USA

ARTICLE INFO

Keywords:
H-terminated nanodiamond
detonation nanodiamond
solvated electron
hydrated electron
advanced reduction processes
perfluoroalkyl substances
PFAS
perfluorooctane sulfonate
perfluorooctane sulfonic acid
PFOS

ABSTRACT

Irradiation of aqueous suspensions containing hydrogen-terminated detonation nanodiamond (HND) with sub-bandgap ($\lambda_{exc} > 225$ nm) excitation leads to the reductive degradation of perfluorooctanesulfonate (PFOS). As evidenced by nanosecond transient absorption spectroscopy (nsTA), we show that 254 nm excitation of HND in water induces the photoemission of electrons producing hydrated electrons (e^-_{aq}). A red shift in the e^-_{aq} absorption maximum relative to bulk water indicates a disruption in the hydrogen bonding network of the interfacial water layer at the HND surface. A shortening of the e^-_{aq} lifetime with the addition of PFOS and accompanying blue shift of the e^-_{aq} absorption maximum indicate PFOS reduction and HND/PFOS surface interactions, respectively. Prolonged photolysis of HND/PFOS solutions at 254 nm results in the degradation of PFOS into smaller poly-fluoroalkyl derivatives consistent with other advanced reduction processes. The degradation of PFOS by this method is less sensitive to pH than the state-of-the-art UV-sulfite method.

1. Introduction

Per- and poly-fluoroalkyl substances (PFAS) are a persistent and recalcitrant class of molecules that are now ubiquitously found in global ground water supplies and soils.[1] Consequently, these substances are recognized by the US Environmental Protection Agency (EPA) and other environmental agencies as environmental contaminants of concern with potential long-term health ramifications.[2] Moreover, the US EPA has recently proposed including perfluorooctanesulfonate (PFOS) and perfluorooctanoate (PFOA) in the Comprehensive Environmental Response, Compensation, and Liability Act of 1980 (CERCLA) list of hazardous substances.

It is, therefore, imperative to develop effective technologies to track and eliminate PFAS contaminants from the environment. This is particularly challenging, however, due to multiple factors including the difficulty of removing PFAS from liquid and solid media, as well as the difficulty in degrading these extremely stable substances. The origin of their stability is their strong C-F bonds, which comprise the hydrophobic backbone of these amphiphilic molecules.

Advanced reductive processes (ARP), [3,4] are considerably more effective at degrading PFAS, such as perfluorooctanoate (PFOA) and perfluorooctanesulfonate (PFOS), as compared to oxidative processes. [5–7] Although PFAS are amenable to reductive degradation, large potential biases are required, making selective electrochemical degradation impractical, particularly in aqueous media.[8,9] ARP in water are typically initiated by UV-irradiation of water-soluble inorganic polyatomic anions and/or organic small molecules resulting in the photoemission of high energy electrons which then solvate. [10,11] Once solvated these electrons are designated as "hydrated electrons", or e^-_{aq}. Hydrated electrons are metastable, having a relatively short lifetime on the order of up to microseconds, and are quite capable of reducing a large number of stable species[12–14] including the recalcitrant C-F bonds in PFAS.[5–7,15–18].

To date, the generation of e^-_{aq} for PFAS degradation by ARP results from UV-irradiation of soluble molecular anions such as sulfite[5–7], iodide[15,16], nitrilotriacetic acid[17], or ethylenediamine tetraacetic acid[18] to name a few examples. The degradative efficiencies in these anionic solutions, however, are limited by factors such as the formation of conjugate acids (for Brönsted-type molecular species at certain pH ranges)[14] or the formation of other reactive photoproducts that actively compete with PFAS for reaction with e^-_{aq}. There is, therefore, a need to develop non-toxic and preferably reusable sources of e^-_{aq} (i.e., photocatalysts) that are less restricted by environmental and mechanistic caveats, while still able to degrade PFAS with high efficiency

* Corresponding author.
E-mail address: william.maza@nrl.navy.mil (W.A. Maza).

https://doi.org/10.1016/j.apcatb.2022.122306
Received 14 October 2022; Received in revised form 15 December 2022; Accepted 17 December 2022
Available online 21 December 2022
0926-3373/Published by Elsevier B.V.

under a wider set of variable environmental conditions. Hydrogen-terminated detonation nanodiamond (HND) as a source of e^-_{aq}[12,13,19,20] exhibits many requisite properties and therefore has the potential to be such an ARP photocatalyst.

HND is a wide bandgap ($E_{bandgap} \sim 5.5$ eV) semiconductor with a conduction band lying ~ 1.1 eV above the vacuum level.[21] As a result, the H-terminated nanodiamond displays negative electron affinity resulting in a near barrier-less ejection of conduction band electrons upon bandgap excitation (i.e. $\lambda_{exc} \leq 225$ nm).[19] Recently, it was reported that HND is capable of photocatalytically initiating reactions with large reduction potentials (e.g. CO_2 reduction and N_2 reduction),[12,13] and offers a large surface area to carry out surface-dependent photocatalytic reactions.[22] Although the underlying mechanism is not fully understood,[23–25] it has also been demonstrated that reductive processes can be effected by solvated electrons generated with sub-bandgap irradiation of H-terminated nanodiamond.[13,26].

Nanodiamond is biocompatible[27] and has been found to exhibit very low cytotoxicity[28] compared to other common e^-_{aq} precursors. Therefore, the UV/HND system has the potential to be an alternative ARP technology for PFAS degradation that is more biologically and environmentally friendly than technologies relying on molecular sources of e^-_{aq}.

Recently, Liu, et al. demonstrated the degradation of PFOA by high energy UV-excitation of HND films grown using chemical vapor deposition.[20] The authors invoked a mechanism in which band-gap excitation of the HND thin-films produced e^-_{aq} for the degradation of PFOA. The authors also suggested, solely based on density functional theory calculations, that surface interactions between PFOA the HND CVD film may have a role in the degradative pathway.

In this report we demonstrate that, in addition to bandgap photoemission, e^-_{aq} are also generated by sub-bandgap irradiation (specifically $\lambda_{exc} = 254$ nm) of suspensions of HND, and that the e^-_{aq} generated in such a manner are also effective in the decomposition of PFOS. We present direct spectroscopic evidence on the microsecond timescale that sub-bandgap (not just < 225 nm) irradiation of HND suspensions also results in the formation of e^-_{aq}. We also present spectroscopic evidence of the effect of PFOS on the lifetime and spectrum of e^-_{aq} generated from HND. This work provides nsTA and XPS evidence of PFOS interactions with the HND surface. LC-MS data from prolonged UV-photolysis of HND/PFOS solutions demonstrate that the photoemission and formation of e^-_{aq} from HND also effectuate the degradation PFOS in aqueous solution.

2. Materials and methods

All commercially obtained materials were used as received unless otherwise stated. Sodium sulfite (Na_2SO_3, Alfa Aesar, 98%), Trizma (Sigma-Aldrich, ≥ 99.9%), potassium ferrocyanide ($K_4Fe(CN)_6$, Sigma-Aldrich, > 99.95%), and potassium perfluorooctane sulfonate salt (PFOS, Sigma-Aldrich, ≥ 98%) were obtained from Sigma Aldrich. Detonation nanodiamond was obtained from Adamas Nanotechnology.

2.1. Preparation of H-terminated nanodiamond (HND)

H-terminated nanodiamond (HND) was prepared from a nanodiamond powder, produced by detonation, and refined by Adamas Nanotechnologies. The source detonation nanodiamond (ND) was a finely dispersed grey powder with a median particle size of about 4 nm, and a surface area of 300 – 400 $m^2\ g^{-1}$. To hydrogenate its surface, 1 g of nanodiamond powder was placed in a quartz boat in a horizontal tube furnace (Lindberg). The temperature was raised in steps from ambient to 450 °C over 15 days under a constant hydrogen flow of 29 sccm and at a pressure of 280 Torr. A slow and prolonged increase in temperature first reduces C═O to C-OH, then at higher temperatures hydroxyl (OH) groups are further reduced to C-H.[29,30] At the end of the 16th day the powder was cooled to 50 °C under a hydrogen atmosphere, transferred to a warm glass jar, sealed with a screw cap, and stored in a dry nitrogen-purged cabinet until used.

2.2. Decomposition of PFOS

Experiments probing the decomposition of PFOS resulting from prolonged irradiation of HND were carried out in a Rayonet RPR-100 photochemical reactor (RPR-2537A) equipped with 16 UV lamps (253.7 nm, 35 W max. output) which surround the reaction solution such that the quartz reaction vessel was illuminated from all sides. The sample solutions were typically comprised of 100 mg HND (unless otherwise stated) suspended in 100 mL deionized water (nanopure filtration system, 18 Ω) containing 30 μM PFOS. The optical thickness of the HND reaction solution ($T = \beta C_{HND} L$[31–34] where β is the specific extinction coefficient of HND in water, C_{HND} is the concentration of HND in the reaction vessel, and L is the diameter of the reaction vessel) was estimated to be T ~ 203 for a round bottom of 5 cm diameter using a β value, as defined by Cabrera, et al.[35], of $4.1 \times 10^4\ cm^2\ g^{-1}$. The optical thickness of the reaction solution is higher than the optimal values predicted for heterogeneous photocatalysts in solution which may limit the PFOS rate of degradation in our photoreactor.[31–34] The experiments were carried out under anaerobic conditions by maintaining a dynamic headspace of N_2 and stirred over the course of the experiment with a magnetic stir bar. Aliquots of the UV-irradiated solutions were collected periodically throughout the course of the experiment to monitor the temporal progression of the PFOS decomposition. These aliquots were passed through inorganic syringe filters (Whatman Anatop, 0.02 μm pore size, 10 mm diameter) and 100 μL portions of these eluents were diluted into 1 mL Nanopure™ deionized H_2O for LC-MS measurements. Degradation of PFOS was quantified by LC-MS using a Varian 500-MS ion trap mass spectrometer with electron spray ionization source in negative ion mode equipped with an Agilent Poroshell 120 C18 Column (3 ×100 mm, 2.7 μm) working in tandem with Varian 212-LC chromatography pumps. The mobile phase for tandem LC-MS measurements was a mixture of 20 mM aqueous ammonium acetate (Solvent A) and 0.1% formic acid in methanol (Solvent B). The initial gradient was 80% Solvent A and 20% Solvent B. This was held for 10 min at a flow rate of 0.3 mL/min at which point the content of Solvent B was increased to 95% for 8 min at the same total flow rate. The content of Solvent B was then decreased to 20% at the same total flow rate for 2 additional minutes. Each run contained a 30 μL injection of the 1 mL sample aliquot taken at various time points over the course of the experiments. LC-MS data was analyzed using the Varian MS Workstation software package. The value of each time point represents the average integrated area of the PFOS 499 *m/z* signal of three separate injections. After each injection, a 30 μL injection of water was passed through the column to minimize sample-to-sample contamination. The integrated 499 *m/z* signal corresponding to PFOS was calibrated to PFOS concentrations by generation of a calibration curve. This curve was obtained using prepared PFOS solutions spanning the concentration range of 50 nM to 50 μM. The *m/z* detection range was 100 *m/z* to 525 *m/z*.

2.3. Nanosecond transient absorption spectroscopy

Transients formed upon UV-light excitation were probed by nanosecond transient absorption (nsTA) spectroscopy carried out on an Edinburgh LP980K system. Suspensions of 0.01 mg/mL in Nanopure™ deionized water were sparging with N_2 for 10 min before the experiment and maintained under a dynamic headspace of N_2 while magnetically stirring throughout the course of the experiment. Suspensions were excited using the ~ 5 ns pulse from an Ekspla NT340B optical parametric oscillator tuned to 254 nm (~ 1 mJ/pulse) and probed in a quasi-colinear configuration with the excitation using a spectrally filtered 150 W Xe flash-lamp. Each transient presented herein represents the average of 30 shots.

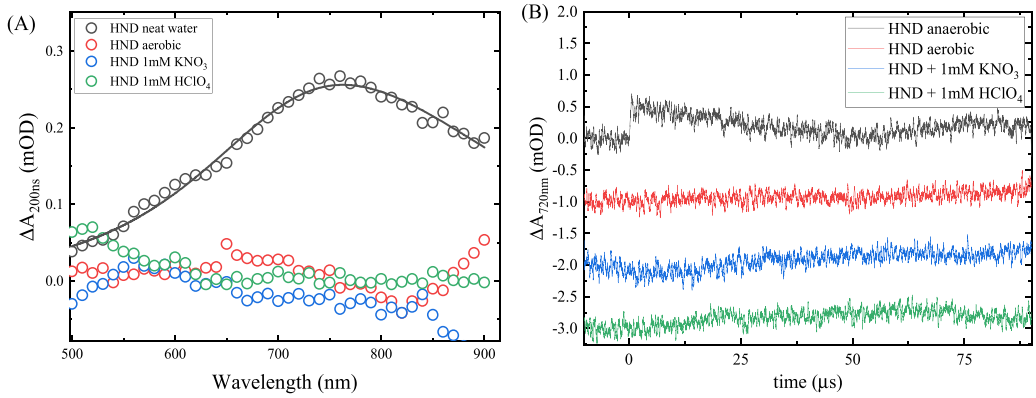

Fig. 1. (A) Transient absorption spectrum obtained 200 ns after the 254 nm excitation pulse and (B) transient decay lifetimes obtained at a 720 nm probe wavelength in solutions containing 0.01 mg/mL HND under anaerobic (black) and aerobic (red) conditions, as well as in the presence of 1 mM KNO_3 (blue), or 1 mM $HClO_4$ (green). The raw data were smoothed by the adjacent averaging of five points. The solid line in (A) represents a best fit of the data to Eqs. 1a and 1b.

2.4. Materials characterization

Changes to the ND surface chemistry were characterized by X-ray photoelectron spectroscopy (XPS). XPS data were acquired using a K-Alpha X-ray Photoelectron Spectrometer (ThermoFisher Scientific). Samples used for XPS measurements were prepared as described above with some exceptions. Suspensions containing 100 mg HND in 100 mL nanopure deionized water and ~ 1.14 mM PFOS (the saturation limit for the potassium salt of PFOS at pH 7) were irradiated for 24 hrs after which the suspensions were centrifuged, the supernatant decanted, and the HND washed with deionized water. This was done four times. The HND was then dried under ambient conditions for XPS analysis. The same was done for samples left in the dark for 24 hrs. The ground-state uv–visible absorption spectrum of a 0.01 mg/mL HND solution was recorded in a 1 cm pathlength quartz cuvette using a Perkin-Elmer Lambda 1050 spectrophotometer. The spectrum was corrected by fitting the raw data in the region between 500 nm and 800 nm using the non-linear curve fitting application in OriginPro 2023 to the function $A = \log\left(\frac{1}{1-a\lambda^n}\right) + b$ where λ is the wavelength. The results of the fit are outlined in the supplemental information (Fig. S1). This was subtracted from the raw data to remove contributions to the absorption spectrum by Mie scattering. The particle size distribution in water was estimated by dynamic light scattering using a DynaPro Nanostar.

3. Results and discussion

3.1. Ground state UV-Visible absorption and particle size distribution

The turbidity of a 0.01 mg/mL HND solution induces light scattering by the incomplete dissolution of the HND, likely due to aggregation of HND in water.[36] Dynamic light scattering indicate HND aggregates form in water with an average diameter ~ 220 nm which is consistent with other reports.[36,37] The steady-state UV–visible absorption spectrum of the same 0.01 mg/mL solution of HND (Fig. S1a) is relatively featureless between 200 nm and 800 nm. The spectrum was corrected for Mie scatter and the resulting corrected absorption displays a band-edge with an intercept at ~ 230 nm (5.4 eV), consistent with the reported 5.5 eV bandgap of HND.[19,21].

3.2. Transient absorption in the presence of e^-_{aq} scavengers

Sub-bandgap excitation of a 0.01 mg/mL solution of HND in neat water at 254 nm produces a transient signal with positive absorbance between 500 nm and 900 nm with an absorption maximum at ~780 nm (Fig. 1A). We attribute this transient signal to e^-_{aq} based on its response to known e^-_{aq} scavengers (vide infra) which is consistent with previous assignments of this feature.[14,38,39] The transient signal (monitored at 720 nm) has a lifetime, τ, of 3.0 ± 0.4 μs under anaerobic conditions (Fig. 1B). Upon excitation of HND at 254 nm, the sensitivity of the nsTA signal to $HClO_4$, KNO_3, and O_2 (Fig. 1A) confirms our assignment of this transient to the formation of e^-_{aq}. It is known that hydrated electrons, e^-_{aq}, can react quickly and reduce a variety of chemical species such as oxygen ($k = 1.9 \times 10^{10}$ M^{-1} s^{-1})[40]. In the presence of oxygen, no e^-_{aq} absorption is observed at 720 nm indicating very fast depletion of the e^-_{aq} occurring within the excitation laser pulse width (< 5 ns, Fig. 1). Similarly, the absorption band is not observed in the presence of 1 mM KNO_3 and 1 mM $HClO_4$, which is consistent with previous reports of e^-_{aq} quenching by nitrate ($k = 1.1 \times 10^{10}$ M^{-1} s^{-1})[40] and protons ($k = 2.3 \times 10^{10}$ M^{-1} s^{-1})[40], respectively.

The nsTA spectral data were fit piecewise to the Gaussian and Lorentzian functions given by Eqs. (1a) and (1b) [41,42] to identify the energy of the absorption maximum in the absence and presence of PFOS.

$$A = A_{max}\exp\left\{-\left[\frac{E - E_{max}}{g}\right]^2 \ln(2)\right\}, E < E_{max} \quad (1a)$$

$$A = \frac{A_{max}}{1 + \left[\frac{E - E_{max}}{l}\right]^2}, E < E_{max} \quad (1b)$$

Here A and A_{max} are the absorbance at a given transition energy (E) and the energy of the absorption maximum (E_{max}), respectively; g and l are related to the full width at half-max at the maximum of the Gaussian and Lorentzian functions, respectively. Results obtained from the fits indicate an absorption maximum centered at ~ 780 ± 12 nm (1.59 ± 0.02 eV) for solutions of HND in neat water. The E_{max} value obtained in the absence of PFOS is bathochromically shifted relative to the 720 nm (1.72 eV) value reported for the E_{max} of e^-_{aq} in bulk water.[42–44] This result supports the model that the hydrogen bonding network of water at the HND-solvent interface is significantly perturbed as previously proposed by Petit, et al.[45] Specifically, a weakening of the hydrogen-bonding network of the water at the HND-solvent interface was proposed, which would result from the presence of hydrophobic regions on the HND surface and it's positive surface ζ-potential.

3.3. Effect of PFOS on the lifetime of the e^-_{aq}

Transient absorption has previously been used to probe changes in e^-_{aq} lifetimes in the presence of PFAS (including PFOS and PFOA).[18,38,39,46] The rate expression that describes the observed decay rate (k_{obs}) at a given [PFOS] and corresponds to the initial reduction of PFOS monomers by e^-_{aq} according to Eq. (2a).

$$PFOS^- + e^-_{aq} \xrightarrow{k_1} product \quad (2a)$$

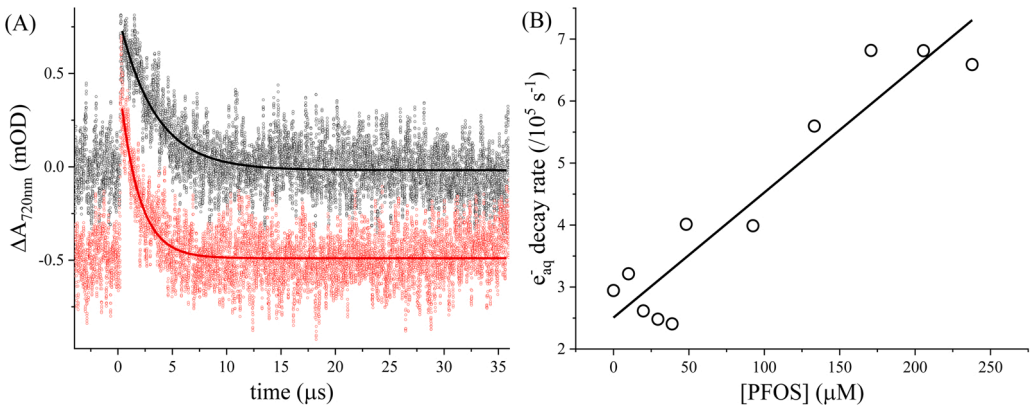

Fig. 2. (A) The e^-_{aq} lifetime decays in the absence (black) and presence (red) of 250 μM PFOS obtained at $\lambda_{exc} = 254$ nm and $\lambda_{probe} = 720$ nm. The signals are offset by 0.5 mOD for clarity. Solid lines indicate best fits to the data using a monoexponential decay model. (B) The e^-_{aq} decay rate obtained from nsTA as a function of [PFOS] for a solution of 0.01 mg/mL HND in neat water.

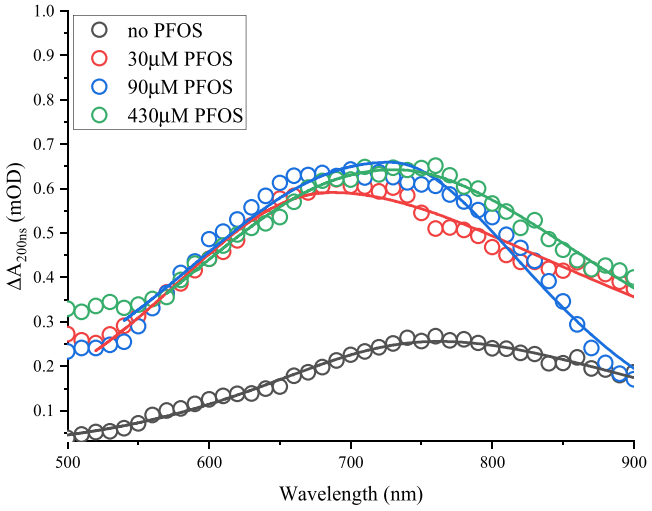

Fig. 3. Transient absorption spectra of solutions containing 0.01 mg/mL HND in neat water (black), and in the presence of 30 μM (red), 90 μM (blue), and 430 μM PFOS (green) 200 ns after the excitation pulse. The raw data were smoothed by the adjacent averaging of five points. The solid lines represent non-linear squares fits of the data to the model given by Eqs. (1a) and (1b) in the text [42].

is given by Eq. (2b).

$$k_{obs} = k_o + k_1[PFOS] \quad (2b)$$

Here, k_o and k_1 are the natural decay rate constants of the e^-_{aq} in the absence of PFOS and the rate constant describing the reaction between e^-_{aq} and PFOS monomers according to Eq. (2a), respectively. The reaction between e^-_{aq} and PFOS occurs on the microsecond timescale and has been assigned by others as a reductive defluorination.[46–48] We have previously reported this reaction to have a pseudo-first order rate constant of $\sim 2 \times 10^9$ M^{-1} s^{-1}.[38] The decay rate of the transients obtained at 720 nm for solutions of HND increases in the presence of > 50 μM PFOS (Fig. 2A) such that the e^-_{aq} lifetime decreases from ~ 3.0 μs to ~ 1.5μs in the presence of 250 μM PFOS. A fit of the decay rate vs. [PFOS], Fig. 2B, results in an observed rate constant k_1 of (1.7 ± 0.9) x10^9 M^{-1} s^{-1} according to Eq. 2b, which is in good agreement with what we previously reported for PFOS in solutions of ferrocyanide.[38].

3.4. Surface interaction of PFOS and HND

Interestingly, the decreased rate of decay in the presence of PFOS is accompanied by an increase in signal amplitude (Fig. 3B). The initial amplitude is directly proportional to the concentration of e^-_{aq} formed within the laser pulse, therefore, the addition of PFOS results in an increased e^-_{aq} yield from 254 nm excitation of HND. The origin of the increased e^-_{aq} yield is uncertain but may, at least in part, be related to interactions between PFOS and the HND surface as has been suggested, but not verified, by Liu, et al.[20] for PFOA and HND CVD thin films. Interactions between surfactants and HND surfaces have also been probed by others.[49,50] For example, Vervald, et al.[36] observed a decrease in HND aggregate size and ζ-potential in water upon addition of octanoate, a non-fluorinated analogue of PFOA, suggesting the presence of surface interactions between HND and surfactants; the authors proposed that at concentrations of octanoate below the critical micelle concentration (CMC, between 300 and 360 mM [51]) these surface interactions can occur between both the surfactants ionic head group and the HND positively charged surface as well as between hydrophobic regions on the HND surfaces and the surfactant hydrocarbon tail. Above the CMC, the authors asserted that the latter was the dominant interaction, i.e., between hydrophobic regions on the HND and the hydrocarbon tail of the surfactant. Vervald, et al.[50] also demonstrated an increase in fluorescence emission intensity of HND particles in the presence of both cationic and anionic surfactants, proposing that the increased fluorescence is due to restricted access of H_2O to the HND surface as a result of surfactant adsorption. Petit, et al.[45] have suggested that, due to the hydrophobic nature of the HND surface, upon hydration there is an accumulation of charge at the H_2O-HND interface. Adsorption of PFOS at the HND surface is expected to perturb the hydration at the HND-H_2O interface, further disrupting the hydrogen-bonding network of the H_2O at the HND-H_2O interface, and perhaps also increasing the hydrophobicity of the HND surface, based on the mechanism proposed by Vervald, et al.[36,52].

Perturbation of the H_2O-HND interface due to PFOS adsorption likely induces changes to the local dielectric of the e^-_{aq} which would manifest in a shift of the observed absorption maximum of the e^-_{aq} transient spectrum as the absorption maximum of the solvated electron is known to be dependent on the solvent dielectric.[44,53] Fig. 3 shows the transient absorption spectrum of e^-_{aq} obtained from a 0.01 mg/mL solution of HND in the absence and presence of 30 μM PFOS, 90 μM PFOS, and 430 μM PFOS. A hypsochromic shift in the e^-_{aq} spectrum occurs at 30 μM and 90 μM PFOS, relative to the absence of PFOS, with maxima centered at ~ 707 nm (1.75 eV) and ~ 704 nm (1.76 eV), respectively, based on a spectral fit of the data according to Eqs. 1a and 1b. A bathochromic shift to ~732 nm (1.69 eV) is further observed when the [PFOS] is increased to 430 μM (Fig. 3). It is clear that an interaction between PFOS and the HND indeed occurs based on the observed blue shift of the e^-_{aq} absorption maximum in the presence of PFOS. Moreover, it is also evident that this

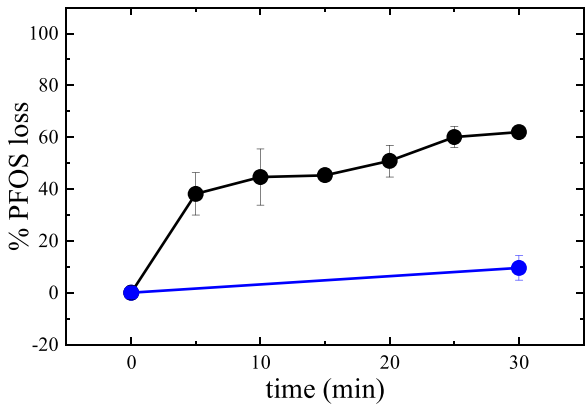

Fig. 4. Time evolution of PFOS loss, based on the loss of the LCMS signal corresponding to the mass of PFOS (499 *m/z*), of solutions containing 1 mg/mL HND in the presence of 30 μM PFOS under 254 nm irradiation (black). The blue data points correspond to 1 mg/mL HND in the presence of 30 μM PFOS incubated in the dark. Experiments were carried out in quartz vessels under N_2 atmosphere.

interaction plays a role in increasing the yield of the photoemission of e^- into the solvent from the HND, as evidenced by the increased signal amplitude.

XPS was used to compare the $F_{1\,s}$, S_{2p}, and O_{2p} XPS signal of the HND surface incubated in the absence and presence of PFOS for 24hrs (Fig. S2). After incubation with PFOS, the HND was recovered by centrifugation and washed thoroughly with deionized water and dried under N_2. New signals present at 292.2 eV and 294.5 eV corresponding to C-F_2 and C-F_3 C1s bond energies, and new signals at 689.4 eV and 169.2 eV corresponding to F1s and S2p respectively confirm the presence of PFOS on the surface of the HND. No observable shifts in the maxima corresponding to the XPS signals were observed with samples exposed to 254 nm irradiation (vide infra, Fig. S2). Additionally, there was no difference observed in the peak positions of the $C_{1\,s}$, $F_{1\,s}$, S_{2p}, and O_{2p} signals after 254 nm irradiation suggesting no change in the surface chemistry of the HND.

3.5. Sub-bandgap irradiation of HND promotes degradation of PFOS

Having established that sub-bandgap irradiation of HND in water results in the photoemission of e^-_{aq}, and that the lifetimes of e^-_{aq} are quenched by PFAS, we now characterize PFOS loss in a photoreactor. We illuminated suspensions containing 1 mg/mL HND and 30 μM PFOS with UV-C irradiation (254 nm) in a quartz flask with stirring under N_2. The concentration of HND was chosen such that the optical density of the HND, after correcting for scattering effects, would be appreciable at 254 nm based on the absorption spectrum shown in Fig. S1. After 30 min irradiation time in un-buffered water, we observed a loss of the LCMS signal corresponding to the molecular mass of PFOS (*m/z* 499, Fig. 4) which is not observed when irradiating PFOS in the absence of HND.

Although the Hg lamps used in the photochemical degradation of PFOS mainly emit at 254 nm, these lamps have additional emission lines throughout the UV (250–400 nm) and visible (400–600 nm) spectral ranges (Fig. S3). Therefore, to identify that the photochemical degradation observed is a consequence of UV-C irradiation (< 280 nm) and not wavelengths > 280 nm, a 1 mg/mL HND solution containing 30 μM PFOS was irradiated in a Pyrex flask, which filters out light of λ < 300 nm. We observed negligible loss of PFOS over the course of 30 min of irradiation in Pyrex vessels when compared to quartz vessels (Fig. S4) indicating that formation of e^-_{aq} is negligible at λ ≥ 300 nm.

Prolonged UV irradiation of un-buffered aqueous solutions containing 1 mg/mL HND and 30 μM PFOS resulted in nearly complete loss of PFOS within 6 hrs (Fig. 5) with an observed overall degradation rate of 0.012 min^{-1}. Analysis of the TIC (total ion count) chromatograms over the progression of the photochemical degradation of PFOS reveal the temporal formation and loss of several products with the following *m/z* (Fig. S5): *m/z* 481, *m/z* 381, *m/z* 331, *m/z* 319, and *m/z* 281. We believe these signals correspond to the PFOS fragments $C_8HF_{16}SO_3^-$, $C_6HF_{12}SO_3^-$, $C_5HF_{10}SO_3^-$, $C_8H_{10}F_5SO_3^-$, and $C_4HF_8SO_3^-$, respectively. The products observed imply the involvement of H/F exchange and chain shortening by C-C bond breaking reactions in the overall degradation of PFOS, processes that have been discussed extensively[54–57] in the context of degradation of PFASs by e^-_{aq}.

Specifically, H/F exchange has been proposed to occur via similar mechanisms for both perfluorinated carboxylates and perfluorinated sulfonates and, in the case of PFOS, involve reductive defluorination of PFOS by e^-_{aq} Eq. (3).

$$C_8F_{17}SO_3^- + e^-_{aq} \rightarrow C_8F_{16}SO_3^{\bullet 3-} + F^- \quad (3)$$

followed by hydrogen abstraction from a neighboring water Eq. (4) [55, 56].

$$C_8F_{16}SO_3^{\bullet 3-} + H_2O \rightarrow C_8HF_{16}SO_3^- + OH^\bullet \quad (4)$$

Alternatively, van Hoomissen and Vyas[57] have suggested that reductive defluorination Eq. (3) and a second reduction by e^-_{aq} Eq. (5).

$$C_8F_{16}SO_3^{\bullet 3-} + e^-_{aq} \rightarrow C_8F_{16}SO_3^{2-} \quad (5)$$

is followed by proton abstraction from neighboring water Eq. (6).

$$C_8F_{16}SO_3^{2-} + H_2O \rightarrow C_8HF_{16}SO_3^- + OH^- \quad (6)$$

Chain shortening by C-C bond breaking has been proposed to involve a secondary reduction by e^-_{aq} Eq. (5) after an initial reductive defluorination Eq. (3) followed by the C-C bond cleavage generating carbanion and olefin sulfonate fragments Eq. (7) [6,16].

$$C_8F_{16}SO_3^{2-} \rightarrow C_3F_7^- + C_5F_9SO_3^- \quad (7)$$

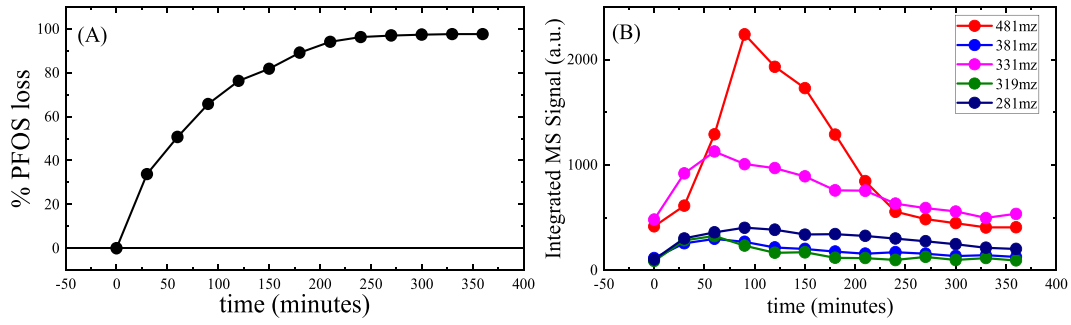

Fig. 5. (A) Time evolution of PFOS consumption, based on the loss of the LC-MS signal corresponding to the mass of PFOS (499 *m/z*), of a solution containing 1 mg/mL HND and 30 μM PFOS under 254 nm irradiation. (B) Formation and consumption of primary PFOS degradation products observed by LC-MS. Total ion count chromatograms are shown in Fig. S5.

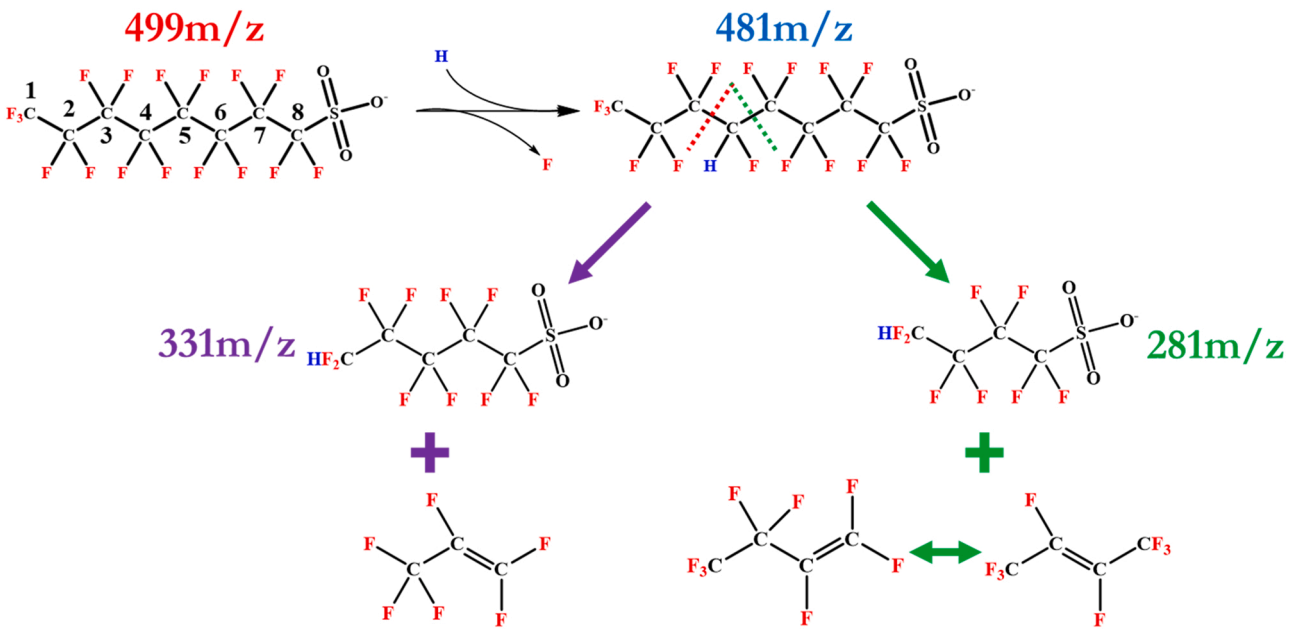

Scheme 1. Fragmentation of PFOS from UV-irradiation of HND as observed by LC-MS.

The example given in Eq. (7) is for the formation of a $C_5F_9SO_3^-$. Our data suggests formation of a perfluorinated olefin and polyfluorinated sulfonate according to Eq. (8) and Eq. (9).

$$C_8F_{16}SO_3^{2-} \rightarrow C_3F_6 + C_5F_{10}SO_3^{2-} \quad (8)$$

$$C_5F_{10}SO_3^{2-} + H_2O \rightarrow C_5HF_{10}SO_3^- + OH^- \quad (9)$$

Reactions (3, 5, 8, and 9) adequately describe the mechanism for the formation of a 331 *m/z* product we observe with LC-MS, which we assign to $C_5HF_{10}SO_3^-$. Formation of $C_5HF_{10}SO_3^-$ agree with theoretical arguments presented by others[56–58] though it is difficult to say from the data here whether $C_6HF_{12}SO_3^-$, $C_5HF_{10}SO_3^-$, or $C_8H_{10}F_5SO_3^-$ is first to form. We believe that similar reactions occur to eliminate C_2F_4, and C_4F_8 respectively resulting in the $C_6HF_{12}SO_3^-$ (*m/z* 381) and $C_4HF_8SO_3^-$ (*m/z* 281) products observed and that the identity of these products is dependent on the C-F site of reduction on the PFOS backbone as has been suggested by others [56,57].

A model is presented in Scheme 1 summarizing the fragmentation of PFOS from UV-irradiation of HND. We will note that the positions of the H-F exchange cannot be determined from the data here; those shown in Scheme 1 are arbitrary. We refer the reader to the excellent theoretical work by others that have identified potential points of H-F exchange for PFASs of varying chain lengths.[56–58] However, the product evolution as a function of time shown in Fig. 5b may suggest C-C bond breaking between C3 and C4, and H-F exchange of lower order PFOS degradative products occurs more readily than H-F exchange of the native PFOS. Notably, recent theoretical work by Biswas, et al.[58] identified C3 and C4 as thermodynamically favorable sites of reduction for PFOS which agrees with previous theoretical work by van Hoomissen and Vyas,[57] and Bentel, et al.[56].

3.6. Degradation of PFOS in HND and the effects of pH

It has been reported that the efficiency of PFOS degradation by a variety of systems capable of forming e^-_{aq} with UV-irradiation (in particular, sulfite, which is now considered the standard) decreases substantially below pH 10.[6,7] A previous investigation demonstrated that the e^-_{aq} lifetime in solutions of sulfite depends on solution pH and the pK_a of bisulfite that forms below pH ~ 9.5.[14] The e^-_{aq} lifetime is less sensitive to pH down to pH 6 in solutions of ferrocyanide (Fig. 6)

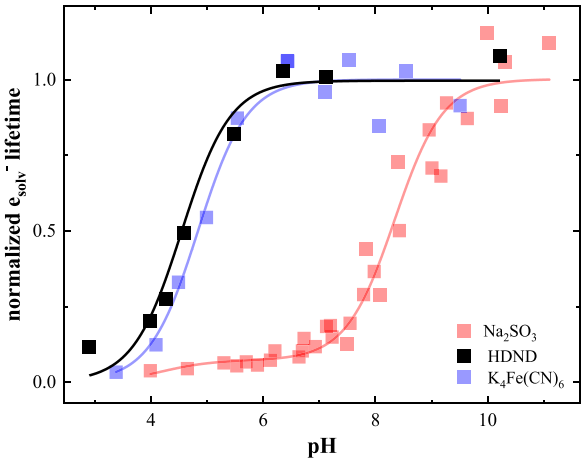

Fig. 6. Dependence on the lifetime of the transients obtained at 720 nm in solutions of HND as a function of solution pH (black squares). The solid black line represents non-linear squares fit of the data to the kinetic model given by Eq. (S7a) in the supplemental (which, in the case of HND reduces to Eq. (3) in the text, vide supra). For comparison, data obtained for the pH dependence on the e^-_{aq} lifetime in solutions of ferrocyanide (blue squares) and sulfite (red squares) are also included. The solid lines represent non-linear squares fits of the data to the generalized kinetic model given by Eq. (S7a) in the supplemental information where B and B^- correspond to SO_3^- and SO_3^{2-} for sulfite, respectively, and $Fe(CN)_6^{3-}$ and $Fe(CN)_6^{4-}$ for ferrocyanide.

whose pK_a is ~ 4.5 compared to that of sulfite (pK_a ~7.2) which is consistent with the high affinity of the Brönsted acid bisulfite (HSO_3^-) for e^-_{aq}.[14] A pH dependence of the e^-_{aq} lifetime was observed in solutions of HND, consistent with the expected reaction of e^-_{aq} with H^+ (Fig. 6). Our results show that in solutions of HND the e^-_{aq} lifetime remains constant down to ~ pH 6 and becomes shorter at pH < 6. This trend suggests the H-terminations of HND are not facilely labile.

The nsTA data in Fig. 6 was fit using a generalized model (Eq. S7a) modified to the present case (Eq. 10) involving HND (derivation in supplemental, see also ref. [14,38]).

$$\frac{\tau_o}{\tau_{obs}} = 1 + k_H \tau_o 10^{-pH} \quad (10)$$

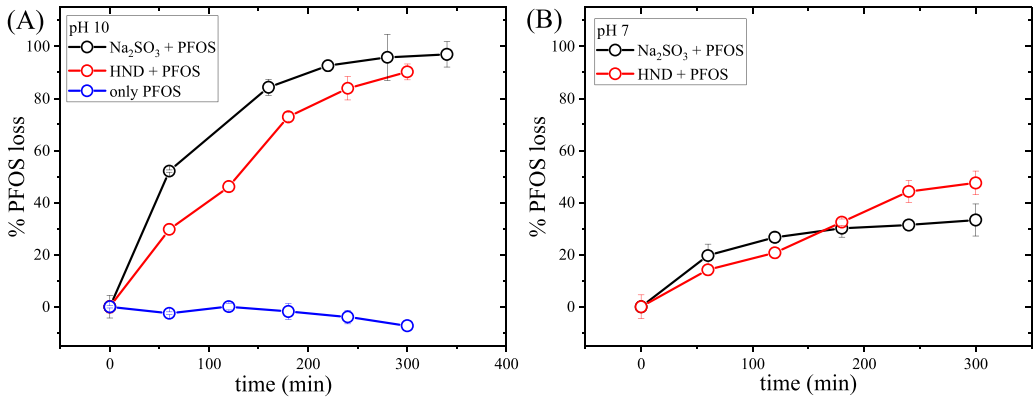

Fig. 7. Time evolution of the loss of PFOS in a solution containing 10 mM trizma and 30 μM PFOS in the absence (blue) and presence of either 10 mM sodium sulfite (black) or 1 mg/mL HND (red), under 254 nm irradiation at pH 10 (A) and pH 7 (B). Total ion count chromatograms are shown in Fig. S6.

Here τ_{obs} and τ_o are the lifetime of the e^-_{aq} at a given pH and at pH ~ 10, respectively, and k_H is the rate constant corresponding to the scavenging of e^-_{aq} by H^+. Results of the fit to Eq. 10 yield a k_H of (3.6 ± 0.9) x10^{10} M^{-1} s^{-1}, which is in good agreement with the accepted rate constant of 2.3 × 10^{10} M^{-1} s^{-1} for scavenging by H^+ [40].

The nsTA results presented above indicate that in solutions of HND the e^-_{aq} lifetime is unaffected by pH down to pH 6 and should effectively reduce PFOS at pH values at which bisulfite competitively inhibits PFOS reduction in solutions of sulfite. Therefore, the effect of pH on the degradation of PFOS in buffered solutions of HND was probed at pH 10 and pH 7 (Fig. 7) and compared to solutions of sulfite. HND solutions were prepared in 10 mM trizma buffer to better control the solution pH throughout the course of the photochemical reaction. The photochemical reaction was also repeated with 10 mM sulfite under the same buffered reaction conditions for comparison. At pH 10, there is an approximate 85% loss of the initial LC-MS signal corresponding to PFOS after 5 hrs of irradiation of the HND solution; similarly, nearly 100% of the initial PFOS signal is lost after 5 hrs of irradiation in sulfite. Alternatively, at pH 7 the reduction in PFOS signal in HND solutions approached ~ 50% displaying a trend towards continued loss of PFOS at longer times whereas in solutions of sulfite the loss of PFOS signal reaches ~ 30% after 10 min with no additional change up to 5 hrs which is consistent with previously reported results.[7] We note that in the protonated form trizma can also behave as a Brönsted acid and, therefore, scavenge e^-_{aq} as previously reported ($k \approx 9 \times 10^6$ M^{-1} s^{-1}).[38] Therefore, the degradative capacity of e^-_{aq} in unbuffered solutions of HND at pH 7 is nearly 100% as shown above in Fig. 5 which is considerably better than the ~ 40% that has been reported for the degradation of PFOS in solutions of sulfite irradiated with VUV-light on a similar time-scale [7].

4. Conclusions

To our knowledge, this work is the first demonstration of the formation of hydrated electrons, e^-_{aq}, in aqueous suspensions of HND nanoparticles using sub-bandgap irradiation of 254 nm with photogeneration of e^-_{aq} that in turn are used to reductively degrade PFOS. XPS and nanosecond transient absorption data is presented to support the presence of surface interactions between PFOS and HND. It is observed that this surface interaction contributes to a greater efficiency in the generation of photoelectrons; however, it is yet unclear whether this interaction contributes to, or facilitates, the degradation of PFOS. This new UV-HND advanced reduction process is shown to be less susceptible to changes in solution pH down to pH 7 than the state-of-the-art UV-sulfite.

Funding

This work was supported by the Office of Naval Research through the U.S. Naval Research Laboratory (Grant # N00014-22-WX-00033).

CRediT authorship contribution statement

William A Maza: Conceptualization, Methodology, Investigation, Writing – original draft, Visualization. **Vanessa M Breslin:** Investigation, Validation, Writing – review & editing. **Tatyana Feygelson:** Investigation, Writing – review & editing. **Paul A DeSario:** Investigation, Writing – review & editing. **Bradford B. Pate:** Conceptualization, Writing – review & editing. **Jeffrey C. Owrutsky:** Conceptualization, Writing – review & editing. **Albert Epshteyn:** Conceptualization, Writing – review & editing.

Declaration of Competing Interest

The authors declare the following financial interests/personal relationships which may be considered as potential competing interests: William A Maza reports financial support was provided by Office of Naval Research.

Data Availability

Data will be made available on request.

Acknowledgements

Support for this work was provided by the Office of Naval Research. WAM and VMB would like to thank the National Research Council for administering their postdoctoral research fellowship for a portion of this work.

Supporting Information

Additional data including derivations of expressions found in the text, ground state uv–visible absorption spectrum and dynamic light scattering particle distribution of HND in water, XPS, as well as additional LC-MS data is available in the Supporting Information associated with this manuscript. This material is available free of charge via the Internet.

Appendix A. Supporting information

Supplementary data associated with this article can be found in the online version at doi:10.1016/j.apcatb.2022.122306.

References

[1] Z.Y. Wang, J.C. DeWitt, C.P. Higgins, I.T. Cousins, A. Never-Ending, Story of per- and polyfluoroalkyl substances (PFASs)? Environ. Sci. Technol. 51 (2017) 2508–2518.

[2] S.E. Fenton, A. Ducatman, A. Boobis, J.C. DeWitt, C. Lau, C. Ng, J.S. Smith, S. M. Roberts, Per- and polyfluoroalkyl substance toxicity and human health review: current state of knowledge and strategies for informing future research, Environ. Toxicol. Chem. 40 (2021) 606–630.

[3] B.P. Vellanki, B. Batchelor, A. Abdel-Wahab, Advanced reduction processes: a new class of treatment processes, Environ. Eng. Sci. 30 (2013) 264–271.

[4] S.Y. Yang, Y.T. Zhang, D. Zheng, Advanced reduction processes: a novel technology for water treatment, Prog. Chem. 28 (2016) 934–941.

[5] Y.R. Gu, T.Z. Liu, Q. Zhang, W.Y. Dong, Efficient decomposition of perfluorooctanoic acid by a high photon flux UV/sulfite process: Kinetics and associated toxicity, Chem. Eng. J. 326 (2017) 1125–1133.

[6] Y.R. Gu, W.Y. Dong, C. Luo, T.Z. Liu, Efficient reductive decomposition of perfluorooctanesulfonate in a high photon flux UV/Sulfite system, Environ. Sci. Technol. 50 (2016) 10554–10561.

[7] Y.R. Gu, T.Z. Liu, H.J. Wang, H.L. Han, W.Y. Dong, Hydrated electron based decomposition of perfluorooctane sulfonate (PFOS) in the VUV/sulfite system, Sci. Total Environ. 607 (2017) 541–548.

[8] J.A. Marsella, A.G. Gilicinski, A.M. Coughlin, G.P. Pez, Selective reduction of saturated perfluorocarbons, J. Org. Chem. 57 (1992) 2856–2860.

[9] A.A. Pud, G.S. Shapoval, V.P. Kukhar, O.E. Mikulina, L.L. Gervits, Electrochemical reduction of some saturated and unsaturated perfluorocarbons, Electrochim. Acta 40 (1995) 1157–1164.

[10] U. Lachish, A. Shafferman, G. Stein, Intensity dependence in laser flash-photolysis experiments - hydrated electron formation from ferrocyanide, tyrosine, and tryptophan, J. Chem. Phys. 64 (1976) 4205–4211.

[11] M.C. Sauer, R.A. Crowell, I.A. Shkrob, Electron photodetachment from aqueous anions. 1. Quantum yields for generation of hydrated electron by 193 and 248 nm laser photoexcitation of miscellaneous inorganic anions, J. Phys. Chem. A 108 (2004) 5490–5502.

[12] L.H. Zhang, R.J. Hamers, Photocatalytic reduction of CO_2 to CO by diamond nanoparticles, Diam. Relat. Mater. 78 (2017) 24–30.

[13] D. Zhu, L. Zhang, R.E. Ruther, R.J. Hamers, Photo-illuminated diamond as a solid-state source of solvated electrons in water for nitrogen reduction, Nat. Mater. 12 (2013) 836–841.

[14] W.A. Maza, V.M. Breslin, N.T. Plymale, P.A. DeSario, A. Epshteyn, J.C. Owrutsky, B.B. Pate, Nanosecond transient absorption studies of the pH-dependent hydrated electron quenching by HSO_3^-, Photochem. Photobiol. Sci. 18 (2019) 1526–1532.

[15] K.E. Yu, X.C. Li, L.W. Chen, J.Y. Fang, H.L. Chen, Q.B. Li, N.P. Chi, J. Ma, Mechanism and efficiency of contaminant reduction by hydrated electron in the sulfite/iodide/UV process, Water Res. 129 (2018) 357–364.

[16] H. Park, C.D. Vecitis, J. Cheng, N.F. Dalleska, B.T. Mader, M.R. Hoffmann, Reductive degradation of perfluoroalkyl compounds with aquated electrons generated from iodide photolysis at 254 nm, Photochem. Photobiol. Sci. 10 (2011) 1945–1953.

[17] Z.Y. Sun, C.J. Zhang, L. Xing, Q. Zhou, W.B. Dong, M.R. Hoffmann, UV/ Nitrilotriacetic acid process as a novel strategy for efficient photoreductive degradation of perfluorooctanesulfonate, Environ. Sci. Technol. 52 (2018) 2953–2962.

[18] P.F. Gu, C.J. Zhang, Z.Y. Sun, H.Z. Zhang, Q. Zhou, S.J. Lin, J.Y. Rong, M. R. Hoffmann, Enhanced photoreductive degradation of perfluorooctanesulfonate by UV irradiation in the presence of ethylenediaminetetraacetic acid, Chem. Eng. J. 379 (2020).

[19] R.J. Hamers, J.A. Bandy, D. Zhu, L. Zhang, Photoemission from diamond films and substrates into water: dynamics of solvated electrons and implications for diamond photoelectrochemistry, Faraday Discuss. 172 (2014) 397–411.

[20] G.S. Liu, C.J. Feng, P.H. Shao, Degradation of perfluorooctanoic acid with hydrated electron by a heterogeneous catalytic system, Environ. Sci. Technol. 56 (2021) 6223–6231.

[21] C.E. Nebel, A source of energetic electrons, Nat. Mater. 12 (2013) 780–781.

[22] Q. Zou, Y.G. Li, L.H. Zou, M.Z. Wang, Characterization of structures and surface states of the nanodiamond synthesized by detonation, Mater. Charact. 60 (2009) 1257–1262.

[23] D. Takeuchi, H. Kato, G.S. Ri, T. Yamada, P.R. Vinod, D. Hwang, C.E. Nebel, H. Okushi, S. Yamasaki, Direct observation of negative electron affinity in hydrogen-terminated diamond surfaces, Appl. Phys. Lett. 86 (2005).

[24] J.B. Cui, J. Ristein, L. Ley, Low-threshold electron emission from diamond, Phys. Rev. B 60 (1999) 16135–16142.

[25] D. Takeuchi, C.E. Nebel, S. Yamasaki, Photoelectron emission from diamond, Phys. Status Solidi A 203 (2006) 3100–3106.

[26] S. Elfimchev, M. Chandran, R. Akhvlediani, A. Hoffman, Visible sub-band gap photoelectron emission from nitrogen doped and undoped polycrystalline diamond films, Appl. Surf. Sci. 410 (2017) 414–422.

[27] Y. Xing, L.M. Dai, Nanodiamonds for nanomedicine, Nanomedicine 4 (2009) 207–218.

[28] L. Moore, J.Y. Yang, T.T.H. Lang, E. Osawa, D.K. Lee, W.D. Johnson, J.Z. Xi, E.K. H. Chow, D. Ho, Biocompatibility assessment of detonation nanodiamond in non-human primates and rats using histological, hematologic, and urine analysis, Acs Nano 10 (2016) 7385–7400.

[29] V.N. Mochalin, O. Shenderova, D. Ho, Y. Gogotsi, The properties and applications of nanodiamonds, Nat. Nanotechnol. 7 (2012) 11–23.

[30] O.A. Williams, J. Hees, C. Dieker, W. Jager, L. Kirste, C.E. Nebel, Size-dependent reactivity of diamond nanoparticles, Acs Nano 4 (2010) 4824–4830.

[31] I. Grcic, G.L. Puma, Photocatalytic degradation of water contaminants in multiple photoreactors and evaluation of reaction kinetic constants independent of photon absorption, irradiance, reactor geometry, and hydrodynamics, Environ. Sci. Technol. 47 (2013) 13702–13711.

[32] I. Grcic, G.L. Puma, Six-flux absorption-scattering models for photocatalysis under wide-spectrum irradiation sources in annular and flat reactors using catalysts with different optical properties, Appl. Catal. B-Environ. 211 (2017) 222–234.

[33] G.L. Puma, A. Brucato, Dimensionless analysis of slurry photocatalytic reactors using two-flux and six-flux radiation absorption-scattering models, Catal. Today 122 (2007) 78–90.

[34] B. Toepfer, A. Gora, G. Li, Puma, Photocatalytic oxidation of multicomponent solutions of herbicides: reaction kinetics analysis with explicit photon absorption effects, Appl. Catal. B-Environ. 68 (2006) 171–180.

[35] M.I. Cabrera, O.M. Alfano, A.E. Cassano, Absorption and scattering coefficients of titanium dioxide particulate suspensions in water, J. Phys. Chem. 100 (1996) 20043–20050.

[36] A.M. Vervald, K.A. Laptinskiy, S.A. Burikov, T.V. Laptinskaya, O.A. Shenderova, I. I. Vlasov, T.A. Dolenko, Nanodiamonds and surfactants in water: Hydrophilic and hydrophobic interactions, J. Colloid Interf. Sci. 547 (2019) 206–216.

[37] H.X. Hu, H.M. Guo, X.Y. Yu, K. Naito, Q.X. Zhang, Surface modification and disaggregation of detonation nanodiamond particles with biodegradable polyurethane, Colloid Surf. A 563 (2019) 302–309.

[38] W.A. Maza, V.M. Breslin, J.C. Owrutsky, B.B. Pate, A. Epshteyn, Nanosecond transient absorption of hydrated electrons and reduction of linear perfluoroalkyl acids and sulfonates, Environ. Sci. Technol. Lett. 8 (2021) 525–530.

[39] W.A. Maza, B.D. Etz, T.C. Schutt, B.L. Chaloux, V.M. Breslin, B.B. Pate, M. K. Shukla, J.C. Owrutsky, A. Epshteyn, Impact of submicellar aggregation on reduction kinetics of perfluorooctanoate by the hydrated electron, Environ. Sci. Technol. Lett. 9 (2022) 226–232.

[40] G.V. Buxton, C.L. Greenstock, W.P. Helman, A.B. Ross, Critical-review of rate constants for reactions of hydrated electrons, hydrogen-atoms and hydroxyl radicals ($^{\cdot}OH/^{\cdot}O^-$) in aqueous-solution, J. Phys. Chem. Ref. Data 17 (1988) 513–886.

[41] F.Y. Jou, G.R. Freeman, Shapes of optical-spectra of solvated electrons - effect of pressure, J. Phys. Chem. 81 (1977) 909–915.

[42] F.Y. Jou, G.R. Freeman, Band resolution of optical-spectra of solvated electrons in water, alcohols, and tetrahydrofuran, Can. J. Chem. 57 (1979) 591–597.

[43] W. Marbach, A.N. Asaad, P. Krebs, Optical absorption of solvated electrons in water and tetrahydrofuran/water mixtures, J. Phys. Chem. A 103 (1999) 28–32.

[44] H.D. Burrows, A correlation of solvated electron absorption-spectra with the solvent parameter Et(30), Radiat. Phys. Chem. 19 (1982) 151–154.

[45] T. Petit, L. Puskar, T. Dolenko, S. Choudhury, E. Ritter, S. Burikov, K. Laptinskiy, Q. Brzustowski, U. Schade, H. Yuzawa, M. Nagasaka, N. Kosugi, M. Kurzyp, A. Venerosy, H. Girard, J.C. Arnault, E. Osawa, N. Nunn, O. Shenderova, E.F. Aziz, Unusual water hydrogen bond network around hydrogenated nanodiamonds, J. Phys. Chem. C. 121 (2017) 5185–5194.

[46] L. Huang, W.B. Dong, H.Q. Hou, Investigation of the reactivity of hydrated electron toward perfluorinated carboxylates by laser flash photolysis, Chem. Phys. Lett. 436 (2007) 124–128.

[47] M. Anbar, Reactions of the Hydrated Electron, Solvated Electron, American Chemical Society, Washington, D.C, 1965, pp. 55–81.

[48] H. Mohan, M. Mudaliar, B. Rao, J. Mittal, Reactions of hydrated electron and alcohol radicals with halogenated aromatic compounds: a pulse radiolysis study, Int. J. Rad. Appl. Instr. C. Rad. Phys. Chem. 40 (1992) 513–517.

[49] G.A. Badun, M.G. Chernysheva, A.V. Gus'kov, A.V. Sinolits, A.G. Popov, A. V. Egorov, T.B. Egorova, I.I. Kulakova, G.V. Lisichkin, Adsorption of alkyltrimethylammonium bromides on nanodiamonds, Fuller. Nanotub. Car. N. 28 (2020) 361–367.

[50] A.M. Vervald, I.V. Plastinin, S.A. Burikov, T.A. Dolenko, Fluorescence of nanodiamonds under the influence of surfactants, Fuller. Nanotub. Car. N. 28 (2020) 83–89.

[51] J.B. Rosenholm, The structure and properties of medium-chain surfactant solutions - a case-study of sodium octanoate, Adv. Colloid Interfac. 41 (1992) 197–239.

[52] A.M. Vervald, I.V. Plastinin, S.A. Burikov, T.A. Dolenko, Fluorescence of nanodiamonds under the influence of surfactants, Fuller. Nanotub. Car. N. 28 (2019) 83–89.

[53] L.M. Dorfman, F. Jou, R. Wageman, Solvent dependence of the optical absorption spectrum of the solvated electron, Berich. Bunsen. Gesell. 75 (1971) 681–685.

[54] J. Cui, P. Gao, Y. Deng, Destruction of per- and polyfluoroalkyl substances (PFAS) with advanced reduction processes (ARPs): a critical review, Environ. Sci. Technol. 54 (2020) 3752–3766.

[55] Y. Qu, C.J. Zhang, F. Li, J. Chen, Q. Zhou, Photo-reductive defluorination of perfluorooctanoic acid in water, Water Res. 44 (2010) 2939–2947.

[56] M.J. Bentel, Y. Yu, L. Xu, Z. Li, B.M. Wong, Y. Men, J. Liu, Defluorination of per- and polyfluoroalkyl substances (PFASs) with hydrated electrons: structural dependence and implications to PFAS remediation and management, Environ. Sci. Technol. 53 (2019) 3718–3728.

[57] D.J. Van Hoomissen, S. Vyas, Early events in the reductive dehalogenation of linear perfluoroalkyl substances, Environ. Sci. Technol. Lett. 6 (2019) 365–371.

[58] S. Biswas, S.C. Yamijala, B.M. Wong, Degradation of per- and polyfluoroalkyl substances with hydrated electrons: a new mechanism from first-principles calculations, Environ. Sci. Technol. 56 (2022) 8167–8175.